Inorganic Chemistry

ARTICLE

pubs.acs.org/IC

Novel Small Stable Gold Nanoparticles Bearing Fluorescent Cysteine−Coumarin Probes as New Metal-Modulated Chemosensors

Elisabete Oliveira,*[,†] Cristina Nuñez,[†,‡] Benito Rodríguez-González,[§] José Luis Capelo,[†,‡] and Carlos Lodeiro*[,†,‡]

[†]BIOSCOPE Group, Faculty of Science, Physical-Chemistry Department, Ourense Campus, University of Vigo, 32004, Ourense, Spain

[‡]REQUIMTE, Department of Chemistry, Faculty of Science and Technology, Universidade Nova de Lisboa, 2829-516 Monte de Caparica, Portugal

[§]Colloid Chemistry Group, CSIC, Campus Lagoas, University of Vigo, 36310, Vigo, Spain

Supporting Information

ABSTRACT: Emissive molecular probes based on amino acid moieties are very appealing because of their application as new building blocks in peptide synthesis. Two new bioinspired coumarin probes (**L1** and **L2**) were synthesized and fully characterized by elemental analysis, infrared, ^{1}H NMR, ^{13}C NMR, UV−vis absorption and emission spectroscopy, matrix-assisted laser desorption-ionization time-of-flight mass spectrometry (MALDI-TOF-MS), lifetime measurements, and X-ray crystal diffraction. Their sensing ability toward alkaline earth, transition, and post-transition metal ions (Ca^{2+}, Zn^{2+}, Cd^{2+}, Cu^{2+}, Ni^{2+}, Hg^{2+}, Ag^{+}, and Al^{3+}) and their acid−base behavior (H^{+}, OH^{-}) were explored in absolute ethanol by absorption and fluorescence spectroscopy. Compound **L1** shows a strong complexation constant with the soft metal ions Zn^{2+}, Cd^{2+}, and Ag^{+}. Compound **L2** shows a high fluorescence quantum yield, and it could be used as a non-pH-dependent fluorescent biological probe. Very small gold nanoparticles (AuNPs) using compounds **L1** and **L2** as stabilizers were obtained by using a reductive method and were characterized by UV−vis, light scattering, and transmission electron microscopy (TEM). Dynamic light scattering and TEM studies show that the formation of small nanoparticles is around 4.27 ± 0.64 nm for **L1** and around 2.69 ± 0.96 nm for **L2**. The new stable Cou@AuNPs behaved as supramolecular chemosensors, which have been selective for the heavy element Hg^{2+}, with a concomitant change of color from pink to dark red/brown and an increase of size up to 100-fold.

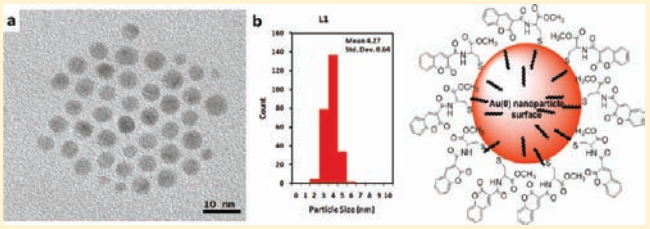

INTRODUCTION

Coumarin is one of the most studied fluorophores because of its interesting photophysical properties. Since the early 1900s, more than 10 000 studies about coumarin derivatives as fluorescent compounds have been published in the literature.[1] Coumarin was first isolated from plants, but it can also be found in microorganisms.[2] Its derivatives have important applications in pharmacology, as an antibacterial, as an anti-HIV, in photochemoterapy, as a stimulant for the central nervous system, as an antioxidant, as an anti-inflammatory, and as anticoagulants with anticancer activity.[3,4] Because of their high capabilities, such as high fluorescent quantum yields and optical properties, they have also been applied as laser dyes, nonlinear optical dyes, fluorescent whiteners, fluorescent probes, and solar energy collectors.[5]

Marschall et al. had reported some cytostatic properties and cytotoxic activity of coumarins,[6] and Reutrakul et al.[7] found two natural coumarins that present cytotoxic activity against mammalian cancer cells. Moreover, Liu et al. had published some novel coumarin derivatives containing a 4,5-dihydropyrazole moiety as a potential active compound against human gastric cancer cells.[8]

Coumarins have interesting properties and applications, especially because of an introduction of an electron-attracting group into the third position and/or an electron repelling group into the seventh position. In both cases this substitution can produce photochemical changes, such as an enhancement of the fluorescent emission.[9] Also, it was proven that the interaction of metals with coordinative groups at the seventh and eighth position in coumarins could enhance their emissive properties as well.

In this way, Thornes and co-workers had published two 6- and 8-subsituent-4-methyl-7-hydroxycoumarins, after which it was discovered that their complexation gave them anticoagulant and plant growth regulating properties.[10] Concerning the application with amino acids, quite recently Kim and co-workers have reported a 7-dimethylamino-coumarin derivative as a fluorescent sensor for homocysteine and cysteine.[11]

New synthetic amino acids with visible excited chromophores are very interesting for bioapplications like fluorescent building

Received: March 31, 2011
Published: August 17, 2011

Scheme 1. Structure of Compounds L1 and L2

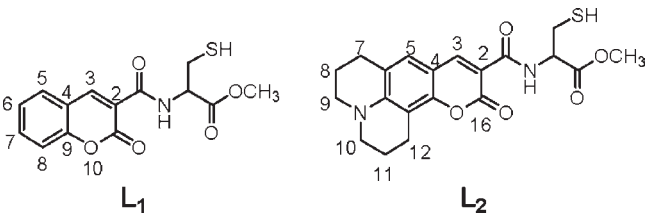

blocks, such as photoinduced electron and energy transfer synthons in long peptides. Some examples are found in the literature involving coumarin and cysteine as biometabolites.[12]

Gold nanoparticles (AuNPs) have been investigated in many fields, such as nanobiotechnology and bioanalytical chemistry.[13] They have been useful in applications such as imaging, catalysis, drug delivery, control of protein activity, understanding a local structure in protein folding, material science, physics, energy, design of nanosensors, and biofuel cells.[14]

AuNPs normally are synthesized by reduction of gold(III) by borohydride/citrate.[15] In order to stabilize the nanoparticles, organic molecules or biomolecules containing thiol (−SH) groups are added to their surface via a gold−thiol bond, preventing their irreversible aggregation. The interaction between chemosensors and nanoparticles could also improve the sensibility of these compounds toward metal ions or other analytes.

To the best of our knowledge, this is the first time that a cysteine amino acid with known reductive properties[16] linked to an emissive coumarin was used to coat gold nanoparticles as a more sophisticated chemosensor system for in vitro and potentially in vivo applications.

Taking into consideration our ongoing projects on fluorescent and colorimetric chemosensors[17] for sensorial[17d,e] and proteomics applications,[17c,f] in this paper we focus on the synthesis of two new emissive coumarin derivatives, **L1** and **L2**, bearing a cysteine as amino acid unit (Scheme 1).

Both compounds were characterized by elemental analysis, matrix-assisted laser desorption-ionization time-of-flight mass spectrometry (MALDI-TOF-MS), ^{1}H and ^{13}C NMR, IR, UV−vis and fluorescence spectroscopy, single crystal X-ray diffraction, and lifetime measurements. Their ability to bind metal ions, such as alkaline, alkaline earth, or transition metal ions, was followed by absorption and emission spectroscopy in absolute ethanol and in mixtures of water/absolute ethanol (80/20 v/v).

Very small stable gold nanoparticles anchoring the compounds **L1** and **L2** were synthesized and characterized by dynamic light scattering (DLS), transmission electron microscopy (TEM), high resolution transmission electron microscopy (HRTEM), and UV−vis spectroscopy. The complexation ability of gold nanoparticles toward heavy metal ions was also investigated.

EXPERIMENTAL SECTION

Physical Measurements. Elemental analyses were carried out with Fisons Instruments EA1108 microanalyzer at the University of Vigo (CACTI), Spain. Infrared spectra were recorded in KBr windows using a JASCO FT/IR-410 spectrophotometer. ^{1}H and ^{13}C NMR were carried out in a Bruker Avance III 400 at an operating frequency of 400 MHz for ^{1}H NMR and 100.6 MHz for ^{13}C NMR using the solvent peak as an internal reference at 25 °C.

Table 1. Crystal Data and Structure Refinement for Compound L1

	L1
empirical formula	$C_{24}H_{13}NO_5S$
formula weight	397.31
temperature	293(2) K
wavelength	0.71073 Å
crystal system	triclinic
space group	*P*1
unit cell dimensions	a = 5.09790(10) Å, α = 99.2530 (10)°
	b = 8.1965(2) Å, β = 104.0090 (10)°
	c = 8.5367(2) Å, γ = 100.3660 (10)°
volume	332.552 (13) Å^3
Z	1
density (calculated)	1.535 g/cm^3
absorption coefficient	0.266 mm^{-1}
F(000)	160
crystal size	0.35 × 0.21 × 0.17 mm^3
θ range for data collection	2.52−25.35°
index ranges	$-6 \le h \le 6$, $-9 \le k \le 9$, $-10 \le l \le 10$
reflections collected	2420
independent reflections	2420 [R(int) = 0.0000]
completeness to θ	100% (25.35°)
absorption correction	none
refinement method	full-matrix least-squares on F^2
data/restraints/parameters	2420/3/199
goodness-of-fit on F^2	1.051
final R indices [$I > 2\sigma(I)$]	$R1$ = 0.0277, $wR2$ = 0.0663
R indices (all data)	$R1$ = 0.0291, $wR2$ = 0.0681
largest diff peak and hole	0.147/−0.207 e Å^{-3}

The MALDI-MS analyses have been performed with a MALDI-TOF-TOF-MS model Ultraflex II (Bruker, Germany) equipped with nitrogen from the BIOSCOPE group, University of Vigo, FCOU-Ourense Campus. Each spectrum represents accumulations of 5 × 50 laser shots. The reflection mode was used. The ion source and flight tube pressure were less than 1.80 × 10^{-7} and 5.60 × 10^{-8} Torr, respectively. The MALDI mass spectra of the soluble samples (1 or 2 μg/μL) were recorded using the conventional sample preparation method for MALDI-MS. One microliter was put on the sample holder on which the ligand had been previously spotted. The sample holder was inserted in the ion source.

Chemicals and Starting Materials. $Ca(CF_3SO_3)_2 \cdot xH_2O$, $Cu(BF_4)_2 \cdot 6H_2O$, $Ni(BF_4)_2 \cdot 6H_2O$, $Zn(BF_4)_2 \cdot xH_2O$, $Cd(CF_3SO_3)_2 \cdot xH_2O$, $Hg(NO_3)_2 \cdot H_2O$, $Ag(BF_4) \cdot xH_2O$, and $Al(NO_3)_3 \cdot 9H_2O$ salts, $HAuCl_4$ (chloroauric acid), CH_3SO_3H (methanosulfonic acid), and hydroxide tetrabutylammonium have been purchased from Strem Chemicals, Sigma Aldrich, or Solchemar. Coumarin-3-carboxylic acid, sodium hydroxide, $KHSO_4$, and magnesium sulfate anhydrous were bought from Aldrich. Thionyl chloride, *N*,*N*′-dicyclohexylcarbodiimide (DCC), and *N*-(tert-butoxycarbonyl)-*S*-benzyl-D-cysteine (Boc-Cys(Bzl)-OH) were bought from Fluka. 1-Hydroxybenzotriazole (HOBt) was bought from Seen Chemicals. Triethylamine was obtained from Aldrich, and coumarin 519 was obtained from Exciton. All compounds were used without previous purification.

Spectrophotometric and Spectrofluorimetric Measurements. Absorption spectra were recorded by a JASCO V-650 spectrophotometer, and a fluorescence emission was recorded by a HORIBA JOBIN YVON FLUOROMAX-4 spectrofluorimeter. The linearity of

the fluorescence emission vs the concentration was checked by the concentration used (10^{-4}–10^{-6} M). A correction of the absorbed light was performed each time that was necessary. The spectrophotometric characterizations and titrations were performed as follows: the stock solutions of the compounds (ca. 10^{-3} M) were prepared by dissolving an appropriate amount of the compounds in a 10 mL volumetric flask and diluting them to the mark with absolute ethanol or water/absolute ethanol (80/20 v/v). The solutions were prepared by appropriate dilution of the stock solutions, which were still 10^{-5}–10^{-6} M. Titrations of the ligands **L1** and **L2** were carried out by the addition of microliter amounts of standard solutions of the ions in absolute ethanol or water. All of the measurements were performed at 298 K.

Luminescence quantum yields were measured using a solution of quinine sulfate in sulphuric acid (0.5 M) as a standard ($[\phi] = 0.54$)[18] for **L1** and an ethanolic solution of acridine yellow G ($[\phi] = 0.47$)[19] for **L2**. Both values were corrected for the refraction index of the solvents.

Lifetime Measurements. Fluorescence decays were measured using a home-built time correlation single photon counting (TCSPC) apparatus as described in other academic papers.[20] The only exception was that a Horiba-JI-IBH NanoLED (λ_{exc} = 339 nm) was used as an excitation source. The fluorescence decays were analyzed using the modulating functions method of Striker et al.[21]

Particles Size Distribution. The nanoparticle size distributions were measured using a dynamic light scattering (DLS) system: a Malvern Nano ZS instrument with a 633 nm laser diode from the Faculty of Science at Ourense Campus, University of Vigo.

TEM Measurements. To perform the transmission electron microscopy (TEM) images, the samples were prepared by dropping 1 μL of the colloidal suspension onto a copper grid coated with a continuous carbon film and allowing the solvent to evaporate. TEM and HRTEM images were obtained through a JEOL JEM 2010F TEM operating at 200 kV. To perform the Fourier transformations, we used the Digital Micrograph (Gatan) software. Data for size distribution histograms were made by measuring more than 200 particles per sample in several TEM images.[22]

X-ray Crystal Structure Determination. Single crystals of compound **L1** were analyzed by X-ray diffraction, and a summary of crystallographic data and the structure refinement parameters are reported in Table 1.

Crystallographic data were collected on a Bruker Smart 1000 CCD diffractometer at CACTUS (University of Santiago de Compostela) at 20 °C using graphite monochromated Mo Kα radiation (λ = 0.71073 Å). Moreover, the crystallographic data were corrected for Lorentz and polarization effects. The SMART[23] software was used to collect frames of data, to index reflections, and to determine lattice parameters. The SAINT[24] software was used to integrate the intensity of the reflections and to scale. The structures were solved by direct methods using the program SHELXS97.[25] All non-hydrogen atoms were refined with anisotropic thermal parameters by full-matrix least-squares calculations on F^2 using the program SHELXL97.[26] Hydrogen atoms were inserted at calculated positions and constrained with isotropic thermal parameters.

Crystallographic data have been deposited at the Cambridge Crystallographic Data Centre: CCDC 730341 for **L1**. Copies of this information may be obtained free of charge from The Director, CCDC, 12 Union Road, Cambridge, CB2 1EZ, U.K. or by fax: +44-1233-336033; by e-mail: deposit@ccdc.cam.ac.uk; or on the Internet at http://www.ccdc.ac.uk.

Synthesis of Organic Ligands. *General Synthesis.* Coumarin-3-carboxylic acid (**A**) (0.30 g, 1.58×10^{-3} mol) (for **L1**) or coumarin 519 (**B**) (0.20 g, 7.01×10^{-4} mol) (for **L2**) were dissolved in freshly distilled dimethylformamide (DMF) (2 mL), and the mixture was cooled in an ice bath, followed by the addition of HOBt (0.21 g, 1.58×10^{-3} mol (**L1**) or 0.09 g, 7.01×10^{-4} mol (**L2**)) and DCC (0.33 g, 1.58×10^{-3} mol (**L1**) or 0.14 g, 7.01×10^{-4} mol (**L2**)). The mixture was stirred in an ice bath for 30 min.

In a separate flask, thionyl chloride (0.16 mL, 2.26×10^{-3} mol) was added dropwise with stirring into methanol (10 mL), and the mixture was cooled in an ice bath, followed by the addition of Boc-Cys(Bzl)OH (0.50 g, 2.26×10^{-3} mol). The solution was refluxed for 2 h. The solvent was evaporated under reduced pressure, yielding an oil. The oil was washed with diethyl ether, leading to a white powder (HCl·H-Cys(Bzl)-OMe) (see Scheme 2).

Further, HCl·H-Cys(Bzl)-OMe (0.27 g, 1.58×10^{-3} mol (**L1**) or 0.12 g, 7.01×10^{-4} mol (**L2**)) was neutralized with triethylamine (0.14 mL, 1.58×10^{-3} mol (**L1**) or 0.07 mL, 7.01×10^{-4} mol (**L2**)) in distilled DMF for 30 min. The solution was filtered, and the filtrate was added to the previous mixture containing compound (**A**) (**L1**) or (**B**)

Scheme 2. General Synthetic Pathway of Compounds L1 and L2

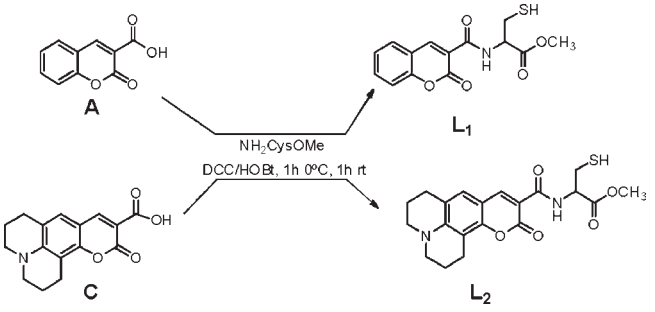

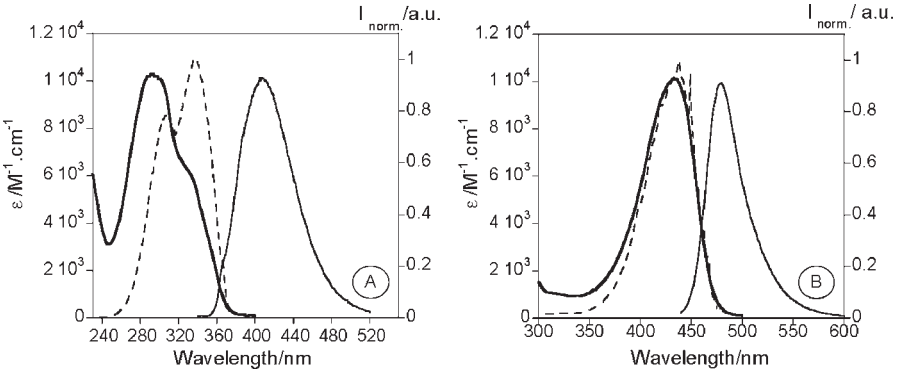

Figure 1. Room temperature absorption (bold line), normalized emission (full line, λ_{excL1} = 330 nm; λ_{excL2} = 435 nm), and excitation spectra (dotted line, λ_{emL1} = 410 nm; λ_{emL2} = 480 nm) of compound **L1** (A) and **L2** (B) in absolute ethanol.

dx.doi.org/10.1021/ic200664z |*Inorg. Chem.* 2011, 50, 8797–8807

Table 2. Photophysical Data of Compounds L1 and L2 in Absolute Ethanol

	UV−vis		fluorescence					
compounds	λ_{exc}(nm)	log ε	λ_{em}(nm)	Stokes' shift (cm^{-1})	quantum yield ϕ	lifetime τ (ns)	K_r 10^8 (s^{-1})	K_{nr} 10^8 (s^{-1})
L1	330	3.80	410	5912	0.02	0.59	0.34	16.6
L2	435	4.00	480	2155	0.41	3.09	1.3	1.9

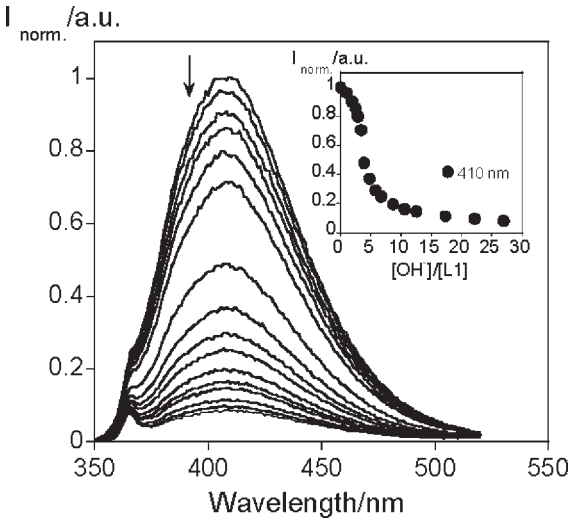

Figure 2. Spectrofluorimetric titration of compound **L1** with the addition of OH^- in absolute ethanol. ([**L1**] = 1.73×10^{-5} M, [OH^-] = 5×10^{-3} M, λ_{exc} = 330 nm, room temperature). Relative standard deviation (RSD) of the values measured at 410 nm was below 10%, n = 3.

(**L2**). The final mixture was stirred for 1 h in an ice bath and 1 h at room temperature. The solvent was evaporated under reduced pressure, and the residue was treated with cooled acetone to remove *N*-acylurea (DCU) from filtration. The solvent was evaporated, and the residue was purified by column chromatography with silica gel (eluent: CH_2Cl_2/MeOH 10:1 (**L1**) or CH_2Cl_2/MeOH 10:5 (**L2**)). The fractions were combined and the desired products **L1** and **L2** were obtained as solid.

L1. White powder (0.29 g, 60%): $C_{14}H_{13}NO_5S \cdot C_4H_{10}O$. FW = 381.44 g/mol.

Elemental analysis. Found: C, 56.7; H, 5.9; N, 4.7; S, 7.4%. CHNS requires: C, 57.0; H, 5.5; N, 4.5; S, 7.7%.

IR (KBr windows) cm^{-1}: ν (NH st) (cm^{-1}) = 3304; ν (alkyl-CH st) (cm^{-1}) = 2924, 2847; (S−H st) (cm^{-1}) = 2541; ν (C═O lactone st) (cm^{-1}) = 1721; ν (C═O st carboxylic acid) (cm^{-1}) = 1705; ν (C═C benzene st) (cm^{-1}) = 1647, 1435, 1308, 1241; ν (N—C═O st) (cm^{-1}) = 1558; ν (C−O−C cyclic ethers st) (cm^{-1}) = 1225, 1213; ν (S−C st) (cm^{-1}) = 750.

NMR spectra: δ_H (DMSO, 400 MHz) ppm: 3.01−3.04 (m, 2H, β-CH_2 Cys), 3.70 (s, 3H, OCH_3), 4.87−4.88 (m, 1H, α-H Cys), 7.71−7.79 (m, 2H, H6, H7), 8.0−8.08 (m, 2H, H5, H8), 8.92 (s, 1H, H3), 9.30−9.32 (d, J = 8 Hz, 1H, NH Cys); δ_C (DMSO, 100 MHz) ppm: 32.35 (C-βCH_2), 52.50 (OCH_3), 54.23 (αC), 128.47 (C6), 130.45 (C5), 131.98 (C7), 134.43 (C8), 144.25 (C3), 160.93 (C═O amide carbonyl).

UV−vis in absolute ethanol (λ nm): bands at 295 nm (log ε = 4.03), 333 nm (log ε = 3.80).

Emission spectrum in absolute ethanol (λ_{exc} = 330 nm, λ_{emis} = 410 nm).

MALDI-TOF-MS (m/z) calc. (found): [**L1**H]$^+$ 308.3 (308.2), [**L1** − **L1**H]$^+$ 613.6 (613.37).

L2. Orange powder (0.067 g, 25%): $C_{24}H_{32}N_2O_6S \cdot C_4H_{10}O$. FW = 476.58 g/mol.

Elemental analysis. Found: C, 60.9; H, 6.3; N, 5.5; S, 6.4%. CHNS requires: C, 60.5; H, 6.7; N, 5.8; S, 6.7%.

IR (KBr windows) cm^{-1}: ν (NH st) (cm^{-1}) = 3320; ν (alkyl-CH st) (cm^{-1}) = 2925, 2848; ν (C═O lactone st) (cm^{-1}) = 1715; ν (C═O st carboxylic acid) (cm^{-1}) = 1684; ν (N—C═O st) (cm^{-1})= 1570; ν (C═C benzene st) (cm^{-1}) = 1621, 1435, 1315, 1240; ν (C−O−C cyclic ethers st) (cm^{-1}) = 1249,1241.

NMR spectra: δ_H ($CDCl_3$, 400 MHz) ppm: 2.62−2.74 (m, 2H, β-CH_2 Cys), 2.85−2.88 (m, 2H, H12), 3.22−3.33 (m, 4H, H11−H7), 3.47−3.58 (m, 6H, H8, H9, H10), 3.78 (s, 3H, OCH_3), 5.02−5.08 (m, 1H, α-H Cys), 6.96 (s, 1H, H5), 8.53 (s, 1H, H3), 9.47−9.51 (m, 1H, NH Cys); δ_C ($CDCl_3$, 100 MHz) ppm: 20.18, 20.41 (C8, C11), 24.96 (C12), 25.63 (C7), 50.02 (C9, C10), 33.97 (C-βCH_2), 52.48 (OCH_3), 54.25 (αC), 130.45 (C5), 144.02 (C3), 159.23 (C═O amide carbonyl).

UV−vis in absolute ethanol (λ nm): bands at 435 nm (log ε = 4.00).

Emission spectrum in absolute ethanol (λ_{exc} = 435 nm, λ_{emis} = 480 nm).

MALDI-TOF-MS (m/z) calc. (found): [**L2** − **L2**H]$^+$ 825.6.

Synthesis of Gold Nanoparticles. Following the Brust[27] methodology, 0.1230 mmol of $HAuCl_4$ was dissolved in 10 mL of mili-Q water, giving a yellow solution, and 0.54 mmol of tetraoctylammonium bromide (98%) as phase transfer (PT) was dissolved in 10 mL of CH_2Cl_2. One milliliter of the gold solution was added to 1 mL of CH_2Cl_2 solution of PT. The mixture was stirred until the water phase was decoloured and the organic phase made deep red by the complete phase transfer of the gold ions. The two solutions were then separated, and 0.0088 mmol of **L1** or **L2** plus 1.2 μL of decanethiol were added to the organic phase, and 1 mL of milli-Q water containing 1.1 mmol of $NaBH_4$ was stirred into the solution, leading to the reduction of the [$AuCl_4^-$] ions. In this case, the autoreductive effect of the cysteine helps nanoparticle formation, causing a color change from red to brown that confirmed the formation of very small stable gold nanoparticles.

The solution of nanoparticles was extracted three times with water, isolated via precipitation with methanol, and centrifuged at 4000 rpm. The absence of free ligands **L1** and **L2** in the final product was confirmed by the lack of their natural fluorescence. Both nanoparticles are very stable in solution, and they maintain their size and color for 4 months.

Gold Nanoparticles Decorated with ***L1***. Color: dark red. UV−vis in dichloromethane (λ, nm): 520. Dynamic light scattering: 3.3 ± 1.1 nm. TEM: 4.27 ± 0.64 nm.

Gold Nanoparticles Decorated with ***L2***. Color: dark red. UV−vis in dichloromethane (λ, nm): bands at 500. Dynamic light scattering: 2.6 ± 1.2 nm. TEM: 2.69 ± 0.96 nm.

RESULTS AND DISCUSSION

Synthesis. Compounds **L1** and **L2** were synthesized by an easy classical solution peptide method using as precursors coumarin-3-carboxylic acid (**A**) for **L1** and coumarin-519 (**B**) for **L2** in the presence of HOBt and DCC, followed by the addition of NH_2-Cys(Bzl)OCH_3. The final products, **L1** and **L2**, were purified by chromatography columns, yielding

dx.doi.org/10.1021/ic200664z |*Inorg. Chem.* 2011, 50, 8797–8807

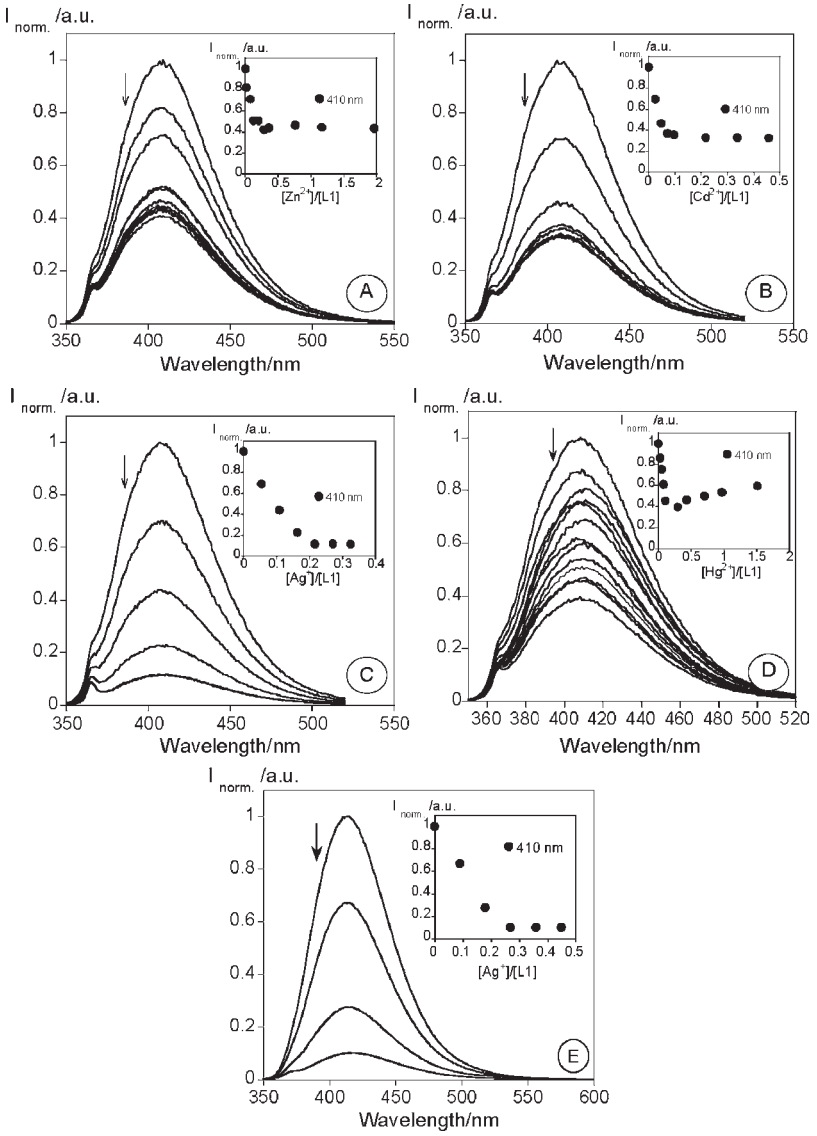

Figure 3. Spectrofluorimetric titration of compound **L1** in the presence of Zn^{2+} (A), Cd^{2+} (B), Ag^{+} (C), and Hg^{2+} (D) in absolute ethanol and in the presence of Ag^{+} (E) in a mixture of water/absolute ethanol (80:20). ($[\mathbf{L1}]_{ethanol} = 1.73 \times 10^{-5}$ M, $[\mathbf{L1}]_{water/ethanol} = 2.23 \times 10^{-5}$ M, $\lambda_{exc} = 330$ nm, room temperature). Relative standard deviation (RSD) of the values measured at 410 nm was below 10%, $n = 3$.

Scheme 3. Coordination Proposed for Zn^{2+}, Cd^{2+}, and Ag^{+} Ions with Compound L1[a]

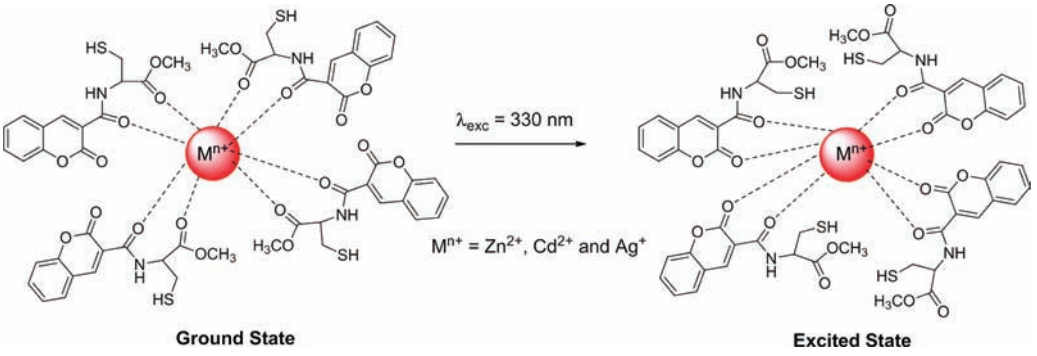

[a] Upon irradiation, a reorganization of **L1** takes place.

60% of a white powder (**L1**) and 25% of an orange powder (**L2**) (Scheme 2).

Both ligands were characterized by elemental analysis, ^{1}H and ^{13}C NMR, infrared in KBr discs, UV−vis and emission

dx.doi.org/10.1021/ic200664z |Inorg. Chem. 2011, 50, 8797–8807

spectroscopy, MALDI-TOF-MS spectrometry, single X-ray diffraction in the case of **L1**, fluorescence quantum yields, and lifetime measurements. The MALDI-TOF-MS spectra of **L1** and **L2** show peaks of the monomeric species $[\mathbf{L1}H]^+$ (308.14 m/z) and the dimeric species $[\mathbf{L1} - \mathbf{L1}H]^+$ (613.37 m/z) for **L1** and of the dimeric species $[\mathbf{L2} - \mathbf{L2}H]^+$ (825.6 m/z) for **L2**.

Table 3. Stability Constants[a] with Free Compounds L1 and L2 in Absolute Ethanol[b]

compounds	**L1** (L:M)	**L2** (L:M)
Zn^{2+}	22.30 ± 0.01 (4:1)	3.04 ± 0.01 (1:1)
Cd^{2+}	21.77 ± 0.01 (4:1)	
Ni^{2+}		4.07 ± 0.01 (1:1)
Ag^{+}	20.34 ± 0.01 (4:1)	
Ag^{+} [c]	22.09 ± 0.02 (4:1)	
Al^{3+}		2.88 ± 0.01 (1:1)
Cu^{2+}		10.63 ± 0.02 (1:1)

[a] log β. [b] By the HypSpec program. [c] In 80/20 (v/v) water/absolute ethanol.

The IR spectra of compounds **L1** and **L2** show bands at ca. 3300 cm^{-1}, assignable to the amide NH; ca. 1720 cm^{-1}, related to the carbonyl of the lactone; 1680−1720 cm^{-1}, where the carbonyl corresponding to the carboxylic acid appears; and 1560 cm^{-1}, which is the band corresponding to the amide N—C═O.

The ^{1}H NMR spectra of ligands **L1** and **L2** present all the characteristic signals of the amino acid backbone NH, α-H, β-CH_2 side chain (for cysteine), and β-CH_3 groups.

In the ^{13}C NMR spectra, the formation of the amide linkage was also confirmed by the appearance of the signal due to the amide carbonyl group at about 148−150 ppm.

Photophysical Studies. The photophysical characterization of compounds **L1** and **L2** was performed in absolute ethanol or in water/absolute ethanol (80/20 v/v) at 298 K. The absorption and emission bands of the coumarin were centered around 330 and 410 nm (Figure 1A) for **L1** and around 435 and 480 nm for **L2** (Figure 1B).

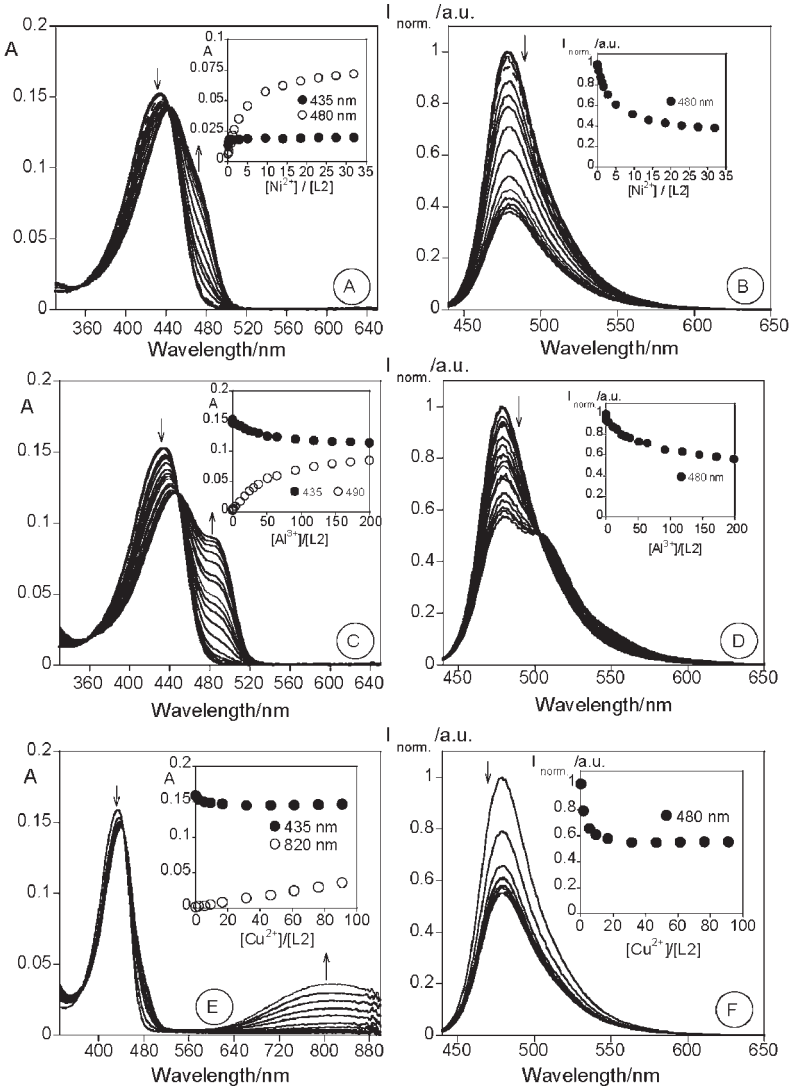

Figure 4. Spectrophotometric and spectrofluorimetric titration of compound **L2** in the presence of Ni^{2+} (A), (B); Al^{3+} (C), (D); and Cu^{2+} (E), (F) in absolute ethanol. ($[\mathbf{L2}] = 1.49 \times 10^{-5}$ M, $[Ni^{2+}] = 1 \times 10^{-2}$ M, $[Al^{3+}] = 3 \times 10^{-2}$ M, $[Cu^{2+}] = 1.7 \times 10^{-2}$ M, $\lambda_{exc} = 435$ nm, room temperature). Relative standard deviation (RSD) of the values measured at 435, 480 nm for absorption and for emission at 480 nm were below 10%, $n = 3$.

dx.doi.org/10.1021/ic200664z |*Inorg. Chem.* 2011, 50, 8797–8807

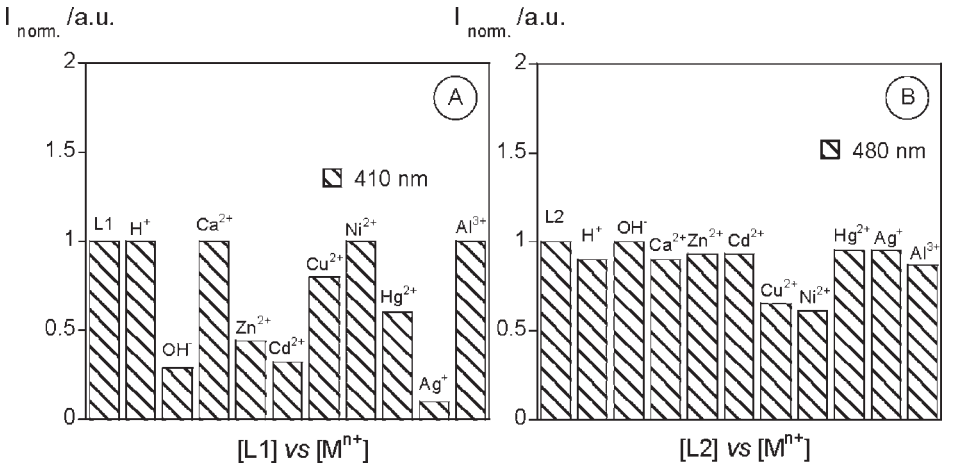

Figure 5. Normalized fluorescence of compounds **L1** (A) and **L2** (B) in the presence of H^+, OH^-, Ca^{2+}, Zn^{2+}, Cd^{2+}, Cu^{2+}, Ni^{2+}, Hg^{2+}, Ag^+, and Al^{3+} in absolute ethanol.

Scheme 4. General Synthetic Pathway for Gold Nanoparticles with L1

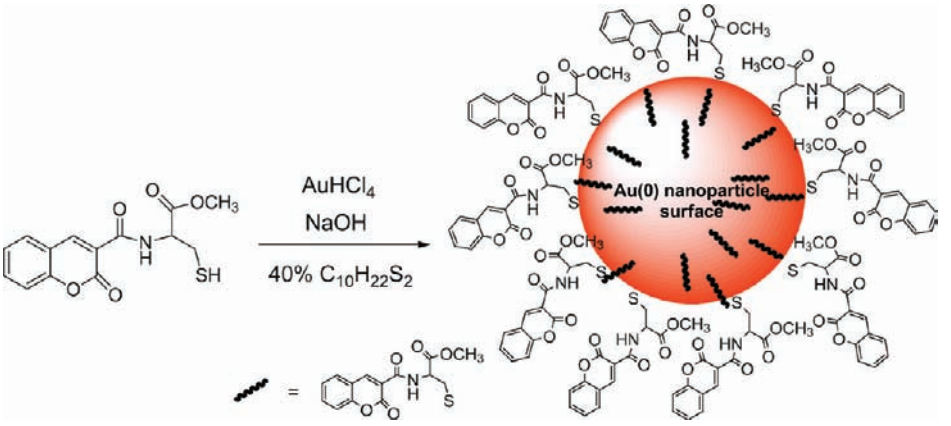

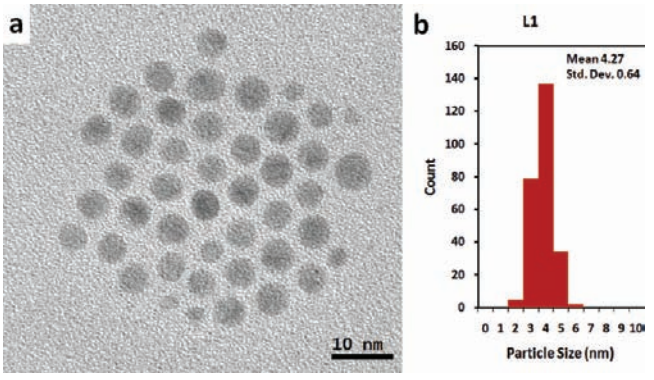

Figure 6. (a) TEM image of sample **L1**; note the regular separation between the particles. (b) Size histogram of an **L1** sample showing a very narrow distribution and a mean diameter of 4.27 nm.

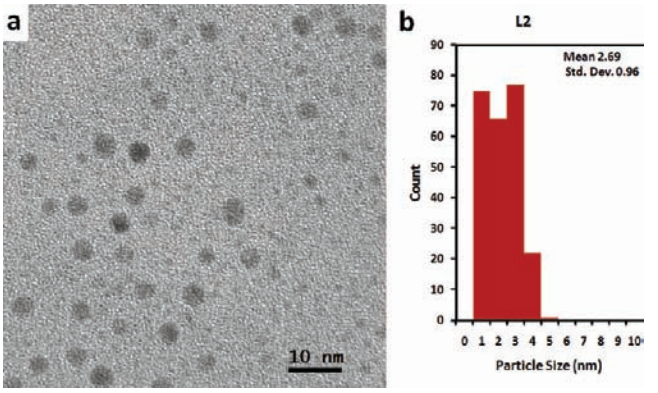

Figure 7. (a) TEM image of sample **L2**. (b) Size histogram of an **L2** sample showing smaller particles and thicker distribution than **L1** sample; mean diameter is 2.69 nm.

In both cases, the absorption band can be assigned to the $\pi-\pi^*$ transition centered on the chromophore units. The perfect match between the absorption and the excitation spectra for compound **L2** rules out the presence of any emissive impurity. Moreover, for compound **L1**, the excitation spectrum is red-shifted in comparison with the absorption spectrum, which might result in the formation of a different species in the excited state, postulated by the high value of the nonradiative decay constant observed ($K_{nr} = 1.66 \times 10^9\ s^{-1}$).

dx.doi.org/10.1021/ic200664z |*Inorg. Chem.* 2011, 50, 8797–8807

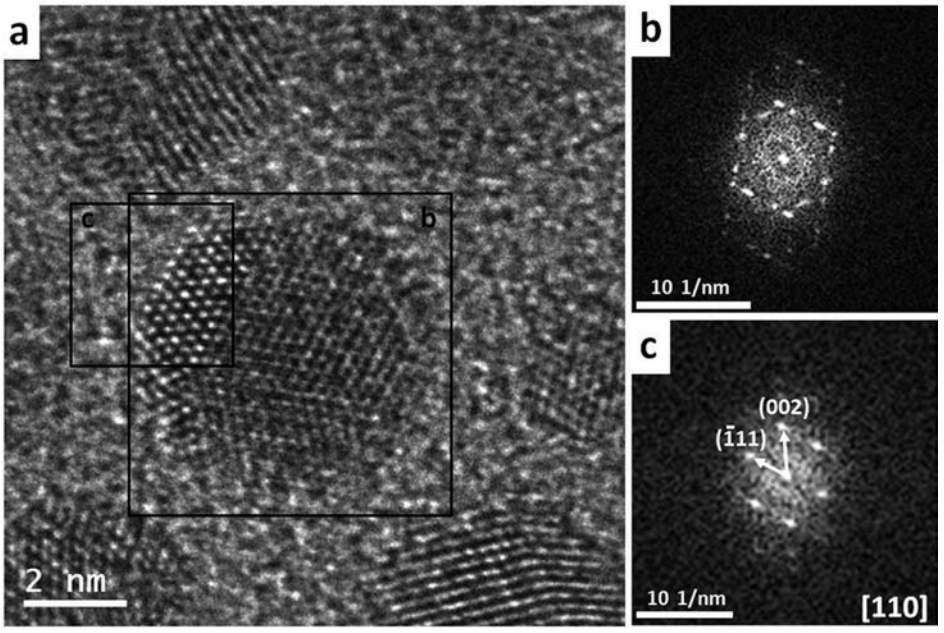

Figure 8. (a) High resolution transmission electron microscopy (HRTEM) image of sample **L1** showing the lattice image of the particles. (b) Fourier transform of the area squared off as "b" in (a); the complex patterns are coming from the polycrystalline nature of the particle. (c) Fourier transform of the area squared off as "c" in (a); the indexation was made using the crystallographic data of the fcc metallic gold.

The relative quantum yields of the compounds **L1** and **L2** were measured in absolute ethanol, using as a reference quinine sulfate and acridine yellow G, respectively.[15,16] Compound **L2**, with a quantum yield of 0.41, turned out to be more emissive than **L1** (0.02). As was reported by Kuo and co-workers,[28] the incorporation of a *N*,*N*-dimethylamino group in the seventh position of coumarin enhances its fluorescence emission. For compound **L2**, the presence of a julolidyl ring in positions six and seven makes this compound much more emissive than **L1**.

Both compounds were also characterized by lifetime measurements, showing values of 0.59 and 3.09 ns for **L1** and **L2**, respectively. Taking into account these values and the luminescent quantum yield, the radiative decay (K_r) and nonradiative decay constants (K_{nr}) can be calculated by the following equation:[29]

$$K_r = \frac{\varphi_F}{\tau} \text{ and } K_{nr} = \frac{1}{\varphi_F} - K_r$$

where φ_F is fluorescent quantum yield.

The calculated values for K_r and K_{nr} in both compounds are reported in Table 2, where the nonradiative decay value for compound **L1** is notable. The photophysical characterization is also shown in Table 2.

Spectrophotometric and Spectrofluorimetric Metal Ion Titrations. The sensorial ability of both compounds was carried out in absolute ethanol and in water/absolute ethanol (80/20 v/v) toward Ca^{2+}, Zn^{2+}, Cd^{2+}, Cu^{2+}, Ni^{2+}, Hg^{2+}, Ag^{+}, and Al^{3+} metal ions. The acid−base behavior of **L1** and **L2** was studied with the increasing addition of protons using methanesulfonic acid, CH_3SO_3H, and hydroxide ions as tetrabutylammonium hydroxide. Both compounds do not show any photophysical changes in acid conditions, but in basic media both compounds show an intense emission quenching of fluorescence emission. This is probably due to the deprotonation of the amine group of the amino acid, which produces a photoinduced electron transfer (PET) process from the lone pair of electrons located in the nitrogen atom to the excited chromophore. (See Figure 2 for compound **L1**.)

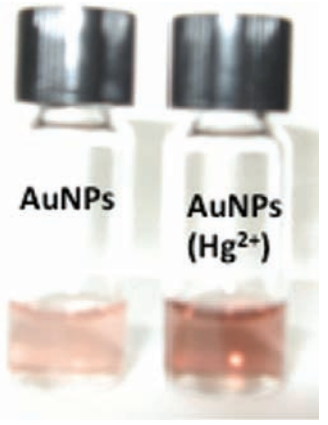

Figure 9. Naked-eye detection of Hg^{2+} by AuNPs@**L1** and after titration with Hg^{2+} in dichloromethane.

The addition of metal ions to compound **L1** in absolute ethanol does not change the ground state, but on the contrary, the excited state is quenched by 0.25 equiv of metal ions (Zn^{2+} (60%), Cd^{2+} (60%), Ag^{+} (90%), and Hg^{2+} (60%)) (Figure 3). This result was also reproduced in a mixture of water/absolute ethanol (80/20 v/v) for Ag^{+} (Figure 3E). However, in the cases of the other metals studied, the quenching was smaller, suggesting stronger competition between water molecules and the ligand. One possible explanation is that in the ground state the metal ion is interacting with the amino acid unit far from the chromophore, then changing its position after the irradiation for the carbonyl of the lactone in the excited state, producing a quenching in the fluorescence emission (Scheme 3).

The stoichiometry of each metal complex was predicted by the Job's plot in which one metal ion is coordinated by 4 equiv of **L1**.

dx.doi.org/10.1021/ic200664z |*Inorg. Chem.* 2011, 50, 8797–8807

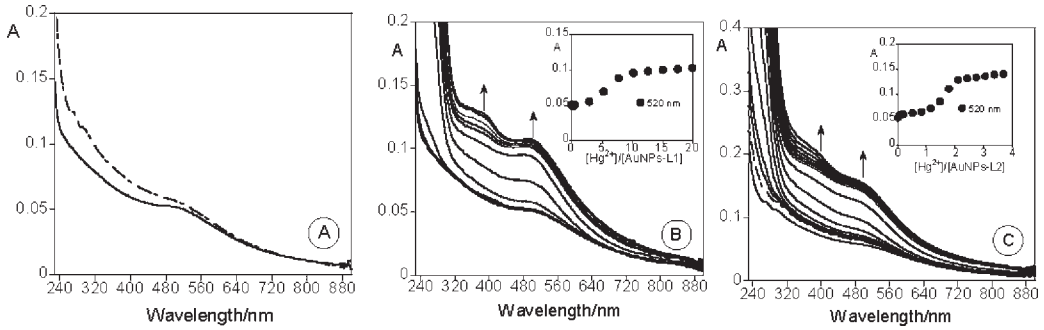

Figure 10. (A) Absorption spectrum of AuNPs with compound **L1** (full line) and **L2** (dotted line). Spectrophotometric titration of AuNPs with compounds **L1** (B) and **L2** (C) with the addition of Hg^{2+} ions in dichloromethane. ([**L1**] = 1.24×10^{-5} M, [**L2**] = 6.35×10^{-6} M, [Hg^{2+}] = 6.01×10^{-3} M, room temperature).

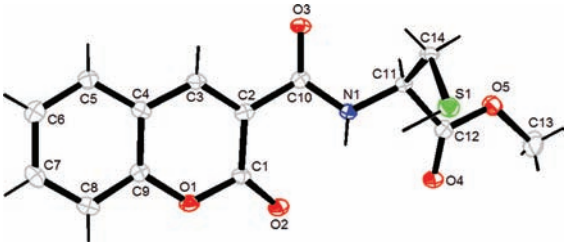

Figure 11. X-ray crystallographic structure of compound **L1** (ellipsoids at 50%).

(Scheme 3). This result is supported by the complexation constants calculated (Table 3) and in comparison with the literature data based on coumarin.[30]

The stability constants obtained from the interaction of compound **L1** derived from coumarin-3 (Table 3) with Zn^{2+}, Cd^{2+}, and Ag^{+} suggest more stable complexes when the metal ionic ratio decreases: $Zn^{2+} > Cd^{2+} > Ag^{+}$.

Compound **L2** does not show any spectral changes in the presence of Cd^{2+}, Ca^{2+}, or Hg^{2+}, while after the addition of Zn^{2+}, Ni^{2+}, Cu^{2+}, and Al^{3+}, it produces notable spectral changes in the ground and excited state. As an example, Figure 4 shows the absorption and emission of **L2** in the presence of Ni^{2+} and Al^{3+}. Other metal ions, such as Zn^{2+} and Cu^{2+}, show the same spectral behavior (data not shown). The complexation constants calculated by using HypSpec[31] for compound **L2** (Table 3) suggest more stable complexes with Cu^{2+} ($\log \beta = 10.63 \pm 0.02$) and Ni^{2+} ($\log \beta = 4.07 \pm 0.01$), followed by Zn^{2+} and Al^{3+} ($\log \beta_{Zn^{2+}} = 3.04 \pm 0.01$; $\log \beta_{Al^{3+}} = 2.88 \pm 0.01$), with a ratio of one metal per one ligand.

The addition of Ni^{2+} or Al^{3+} (Figure 4A,B) produces a decrease in the absorption spectrum at 435 nm, followed by a small red shift of 10 nm, with a concomitant appearance of a new shoulder or band at 480−490 nm. This band appears due to the participation of the carbonyl group in complexation.[32] An isosbestic point for Ni^{2+} and Al^{3+} was observed at 447 and 456 nm, respectively.

According to the formation of a new band at 490 nm and corresponding with the carbonyl−metal ion interaction (Figure 4C), the involvement of the coumarin in the carbonyl group is more intense in $Al^{3+} > Ni^{2+} > Zn^{2+} > Cu^{2+}$.

Comparing both coumarin derivatives, **L1** and **L2**, we can conclude that **L1** is more affected by the metal ion complexation than **L2**. This fact can be observed in the column graph reported in Figure 5.

Synthesis and Characterization of Gold Nanoparticles. The AuNPs coated with compounds **L1** and **L2** were obtained by the Brust[25] methodology on the basis of the reduction with $NaBH_4$ (Scheme 4). The formation of the nanoparticles can be observed because of the appearance of the gold plasmonic resonance band at 520 nm and because of the change in color from orange to red.

These AuNPs were not emissive because the luminescence of the coumarin was totally quenched by the gold metal core. The size of **L1** and **L2** nanoparticles of ca. 3.3 ± 1.1 nm and ca. 2.6 ± 1.2 nm, respectively, was measured by DLS.

It is important to note that by TEM, both samples show very small sizes. The average size observed was 4.27 ± 0.64 nm for **L1**@AuNP and 2.69 ± 0.96 nm for **L2**@AuNP. Actually, TEM images of Figures 6a and 7a show that the particles of the sample **L2** are smaller than **L1** and have a large size dispersion. This difference is also reflected in the histograms of Figures 6 and 7. In the sample **L2**, there are some particles around 4 nm, but in the image (Figure 7a), there is a background of extremely small particles (less than 3 nm) as well. The histogram displays a population peak around 2 nm. We try not to rule out these particles, but they are less than 2 nm in size and are difficult to visualize due to the lack of edge contrast. The shape of the particles is almost spherical and shows no faceted surfaces. It is very remarkable that in both samples, despite the small size, the particles are separated from one another and no significant aggregation is observed. All of this is true, even though the time has not induced overgrowth of the particles and the particles look very stable.

Here we must point out one interesting feature in sample **L1**. As you can see in Figure 6a, when particles are deposited on the TEM grid they are arranged in fairly regular fashion, leaving almost the same distance between them. The separation distance can be explained by taking into consideration the steric effect of the organic molecules attached to the surface of the metallic gold particles. **L1** and **L2** (not shown) samples contain crystalline particles. Figure 8 shows a HRTEM image of the **L1** sample that confirms the existence of crystalline planes within the particles. The Fourier analysis in Figure 8b shows a very complex pattern due to the polycrystalline nature of the particle; most likely this particle is twinned.[19] If the Fourier analysis is performed in an area that corresponds to only one twin (Figure 8c), a single-crystal pattern is obtained. The indexation of the former image confirms that the particles are formed by face-centered cubic (fcc) metallic gold.

Sensing Metal Ions with Gold Nanoparticles. In order to explore the potential application of these functionalized small

dx.doi.org/10.1021/ic200664z |*Inorg. Chem.* 2011, 50, 8797–8807

stable gold nanoparticles (AuNPs) as chemosensors for toxic, heavy, and soft metal ions,[33] Hg^{2+}, Cd^{2+}, Zn^{2+}, and Ag^{+}, several metal titrations were performed following the modifications in the surface plasmonic resonance band (SPRB).

Only in the case of mercury(II) was an effect observed. The addition of Hg^{2+} showed a color change from pink to dark red/brown in both systems (Figure 9), as well as an increase of 100-fold in the nanoparticle size, raising the AuNPs aggregation. The spectrophotometric titration with Hg^{2+} for AuNPs with compound **L1** and **L2** is presented in Figure 10B,C.

On the basis of the Lambert−Beer law and the extinction molar coefficient at 330 and 435 nm for free **L1** and **L2**, respectively, it was possible to determine the approximate concentration of the ligands around each nanoparticle and the concentration of the Hg^{2+} ions. The inset of Figure 10B,C represents the absorption as a function of the number of Hg^{2+} equivalents necessary to stabilize the system. An inspection shows that for the AuNPs@**L2**, 2 equiv of Hg^{2+} are necessary, instead of the 5 equiv for the AuNPs@**L1**. We can conclude that the AuNPs@**L2** is more sensitive to mercury(II) than AuNPs@**L1**.

Crystallography Data. Crystals of compound **L1** (Figure 11) suitable for X-ray diffraction were obtained from the slow evaporation of an ethanolic solution of **L1** at room temperature. The structure is quite planar where the unique remarkable point shows the sulfur atom of the cysteine out of the molecule plane with an angle of 113.99°. Neither hydrogen bond nor $\pi-\pi$ stacking interactions were observed between two adjacent molecules in the crystal packing.

CONCLUSIONS

Two new bioinspired chemosensors, **L1** and **L2**, were synthesized and fully characterized. Both compounds were studied by elemental analysis, MALDI-TOF-MS spectrometry, infrared, lifetime measurements, X-ray crystal diffraction, ^{1}H and ^{13}C NMR, UV−vis absorption and emission fluorescence spectroscopy. Compound **L1** was revealed as being a very good chemosensor for Zn^{2+}, Cd^{2+}, and Ag^{+} soft metal ions, and we postulate that it is a supramolecular complex formed by four ligands around one metal ion. The X-ray structure of **L1** shows a quite planar structure of the ligand. On the other hand, compound **L2** appears to be less sensitive to metal ions, but the highly fluorescent quantum yield that was observed and the stability that is not affected by pH turns **L2** into a very good fluorescent marker for biological applications.

Very small and highly stable gold nanoparticles (AuNPs) were successfully synthesized using both ligands and were studied for the same metal ions. The obtained nanoparticles are about 4.27 ± 0.64 nm and 2.69 ± 0.96 nm in average size and narrow in size dispersion. Both families of particles are stable in solution; no further growth can be seen in it. They are polycrystalline and are made of fcc metallic gold. The presence of molecules on the surface acts as a protection against aggregation and avoids overgrowth. Molecules on the surface also bias the pattern that the particles are deposited on the surface and the distance between them.

The introduction of the nanoparticle core modified the selectivity in both cases, showing an interaction with Hg^{2+} ions, with a change in color from pink to dark red/brown and a 100-fold increase in particle size due to aggregation. With this interesting result, a more sophisticated chemosensor can be constructed on the basis of the triad coumarin−cysteine and AuNPs.

ASSOCIATED CONTENT

Supporting Information. Graphs of emission intensity and absorption data. This material is available free of charge via the Internet at http://pubs.acs.org.

AUTHOR INFORMATION

Corresponding Author

*E-mail: clodeiro@uvigo.es (C.L.), e.oliveira@uvigo.es (E.O.). Fax: + 34 988 387001 (C.L), + 34 988 387001 (E.O.).

ACKNOWLEDGMENT

We are indebted to Xunta de Galiza (Spain) for the Project 09CSA043383PR (Biomedicine). C.L. and J.L. thank Xunta de Galicia for the Isidro Parga Pondal Research Program. The authors thank the Scientific Association Proteomass for financial support. E.O. and C.N. thank the FCT-MCTES (Portugal) for their postdoctoral Grants SFRH/BPD/72557/2010 and SFRH/BPD/65367/2009, respectively, and E. O. thanks Fundação Calouste Gulbenkian for the Prize 2008 in Excellence in Research (Estímulo a criatividade e a qualidade na actividade de Investigação).

We are grateful to Dr. J. Seixas De Melo from the Chemistry Department, Coimbra University for his help with the lifetime measurements.

REFERENCES

(1) (a) Hong, M. L.; Gardecki, J. A.; Maronelli, M. *J. Phys. Chem. A* **1997**, *101*, 1030. (b) Shirota, H.; Segawa, H. *J. Phys. Chem. A* **2003**, *107*, 3719. (c) Kumbhakar, M.; Nath, S.; Mukherjee, T.; Pal, H. *J. Chem. Phys.* **2004**, *120*, 2824. (d) Katerinopoulos, H. E. *Curr. Pharm. Des.* **2004**, *10*, 3835. (e) Seth, D.; Sarkar, S.; Sarkar, N. *J. Phys. Chem. B* **2008**, *112*, 2629. (f) Tasior, N.; Gryko, D. T.; Pielachinska, D. J.; Zanelli, A.; Flamigni, L. *Chem.—Asian J.* **2010**, *5*, 130.

(2) Murray, R. D. H.; Mendez, J.; Brown, S. A. *The Natural Coumarins: Occurrence, Chemistry and Biochemistry*; John Wiley & Sons: New York, 1982.

(3) (a) O'Kennedy, R., Thornes, R. D., Eds.; *Coumarins. Biology, Applications and Mode of Action*; Wiley: Chichester, U.K., 1997. (b) Fylaktakidou, K. C.; Hadjipavlou-Litina, D. J.; Litinas, K. E.; Nicolaides, D. N. *Curr. Pharm. Des.* **2004**, *10*, 3813. (c) Walshe, M.; Howarth, J.; Kelly, M. T.; Kennedy, R. O.; Smyth, M. R. *J. Pharm. Biomed. Anal.* **1997**, *16*, 319. (d) Sardari, S.; Mori, Y.; Horita, K.; Micetich, R. G.; Nishibe, S.; Daneshtalab, M. *Bioorg. Med. Chem.* **1999**, *7*, 1933.

(4) (a) Musa, M. A.; Cooperwood, J. S.; Khan, M. O. F. *Curr. Med. Chem.* **2008**, *15*, 2664. (b) Kostova, I.; Mojzis, J. *Future HIV Ther.* **2007**, *1*, 315. (c) Kostova, I. *Mini-Rev. Med. Chem.* **2006**, *6*, 365.

(5) (a) Jones, G.; Jackson, W. R.; Choi, C.; Bergmark, W. R. *J. Phys. Chem.* **1985**, *89*, 294. (b) Ray, D.; Bharadwaj, P. K. *Inorg. Chem.* **2008**, *47*, 2252. (c) Trenor, S. R.; Shultz, A. R.; Love, B. J.; Long, T. E. *Chem. Rev.* **2004**, *104*, 3059. (d) Hung, T. T.; Lu, Y. J.; Liao, W. Y.; Huang, C. L. *IEEE Trans. Magn.* **2007**, *43*, 867.

(6) Marshall, M.; Kervin, K.; Benefield, C.; Umerani, A.; Albainy-Jenei, S.; Zhao, Q.; Khazaeli, M. *J. Cancer Res. Clin. Oncol.* **1994**, *120*, S3.

(7) Reutrakul, V.; Leewanich, P.; Tuchinda, P.; Pohmakotr, M.; Jaipetch, T.; Sophasan, S.; Santisuk, T. *Planta Med.* **2003**, *69*, 1048.

(8) Liu, X.-H.; Liu, H.-F.; Chen, J.; Yang, Y.; Song, B.-A.; Bai, L.-S.; Liu, J.-X.; Zhu, H.-L.; Qi, X.-B. *Bioorg. Med. Chem. Lett.* **2010**, *20*, 5705.

(9) (a) Griffiths, J.; Millar, V.; Bahra, G. S. *Dyes Pigm.* **1995**, *28*, 327. (b) Azuma, K.; Suzuki, S.; Uchiyama, S.; Kajiro, T.; Santa, T.; Imai, K. *Photochem. Photobiol. Sci.* **2003**, *2*, 443.
(10) Thornes, R. D.; Daly, L.; Lynch, G. *J. Cancer Res. Clin. Oncol.* **2004**, *120*, 32.
(11) Kim, T.-K.; Lee, D.-N.; Kim, H.-J. *Tetrahedron Lett.* **2008**, *49*, 4879.
(12) Eisenbrand, G.; Otteneder, M.; Tang, W. *Toxicology* **2003**, *19*, 249–258.
(13) Cioffi, N.; Palo, F.; Calvano, C.; Werf, D. I.; Palmisano, F.; Zambonin, G. P. *Sens. Lett.* **2008**, *6*, 1.
(14) Aubin-Tam, M.-E.; Hamad-Shifferli., K. *Biomed. Mater. (Bristol, U. K.)* **2008**, *3*, 034001.
(15) Satyabrata, S.; Mandal, T. K. *Chem.—Eur. J.* **2007**, *13*, 3160.
(16) Capelo, J. L.; Lavilla, I.; Bendicho, C. *Anal. Chem.* **2001**, *73*, 3732.
(17) (a) Lodeiro, C.; Capelo, J. L.; Mejuto, J. C.; Oliveira, E.; Santos, H. M.; Pedras, B.; Nuñez, C. *Chem. Soc. Rev.* **2010**, *39*, 2948.(b) Lodeiro, C.; Pina, F. *Coord. Chem. Rev.* **2009**, *253*, 1353. (c) Galesio, M.; Vieira, D. V.; Rial-Otero, R.; Lodeiro, C.; Moura, I.; Capelo, J. L. *J. Proteome Res.* **2008**, *7*, 2097. (d) Mameli, M.; Lippolis, V.; Caltagirone, C.; Capelo, J. L.; Faza, O. N.; Lodeiro, C. *Inorg. Chem.* **2010**, *49*, 8276. (e) Nuñez, C.; Bastida, R.; Macias, A.; Valência, L.; Ribas, J.; Capelo, J. L.; Lodeiro, C. *Dalton Trans.* **2010**, *39*, 7673. (f) Santos, H. M.; Lodeiro, C.; Capelo, J. L. *J. Proteomics* **2010**, *73*, 1411.
(18) (a) Berlman, I. B. *Handbook of Fluorescence Spectra of Aromatic Molecules*, 2nd ed.; Academic Press: New York, 1971. (b) Montalti, M.; Credi, A.; Prodi, L.; Gandolfi, M. T. *Handbook of Photochemistry*, 3rd ed.; Taylor & Francis: Boca Raton, FL, 2006.
(19) Olmsted, J., III *J. Phys. Chem.* **1979**, *83*, 2581.
(20) Seixas de Melo, J.; Fernandes, P. F. *J. Mol. Struct.* **2001**, *565*, 69.
(21) Striker, G.; Subramaniam, V.; Seidel, C. A. M.; Volkmer, A. *J. Phys. Chem. B* **1999**, *103*, 8612.
(22) Sánchez-Iglesias, A.; Pastoriza-Santos, I.; Pérez-Juste, J.; Rodríguez-González, B.; García De Abajo, F.; Liz-Marzán, L. *Adv. Mater. (Weinheim, Ger.)* **2006**, *18*, 2529.
(23) *SMART*, Version 5.054; Bruker Analytical X-ray Systems Inc.: Madison, WI, 1997. Instrument control and data collection software.
(24) *SAINT*, Version 6.01; Bruker Analytical X-ray Systems Inc.: Madison, WI, 1997. Data integration software package.
(25) Sheldrick, G. M. *SHELXS97, A Computer Program for the Solution of Crystal Structures from X-ray Data*; University of Göttingen: Göttingen, Germany, 1997.
(26) Sheldrick, G. M. *SHELXL97, A Computer Program for the Refinement of Crystal Structures from X-ray Data*; University of Göttingen: Göttingen, Germany, 1997.
(27) Brust, M.; Fink, J.; Bethell, D.; Schiffrin, D. J.; Kiely, C. *J. Chem. Soc., Chem. Commun.* **1995**, 1655.
(28) Kuo, P.-Y.; Yang, D.-Y. *J. Org. Chem.* **2008**, *73*, 6455.
(29) Lakowicz, J. R. *Principles of Fluorescence Spectroscopy*, 2nd ed.; Kluwer Academic/Plenum Publishers: New York, 1999.
(30) Grazul, M.; Budzisz, E. *Coord. Chem. Rev.* **2009**, *253*, 2588.
(31) Gans, P.; Sabatini, A.; Vacca, A. *Talanta* **1996**, *43*, 1739.
(32) Santos, H. M.; Pedras, B.; Tamayo, A.; Casabó, J.; Escriche, L.; Covelo, B.; Capelo, J. L.; Lodeiro, C. *Inorg. Chem. Commun.* **2009**, *12*, 1128, and references therein.
(33) Pearson, R. G. *J. Am. Chem. Soc.* **1963**, *85*, 3533.